PERGAMON

International Journal of Heat and Mass Transfer 46 (2003) 221–235

International Journal of HEAT and MASS TRANSFER

www.elsevier.com/locate/ijhmt

Film cooling characteristics of a single round hole at various streamwise angles in a crossflow: Part I effectiveness

C.H.N. Yuen [1], R.F. Martinez-Botas *

Department of Mechanical Engineering, Imperial College of Science, Technology and Medicine, London, SW7 2BX UK

Received 16 November 2001; received in revised form 19 July 2002

Abstract

Film cooling effectiveness were studied experimentally on a cylindrical hole with a streamwise angle of 30°, 60° and 90°, in a flat plate test facility with a zero pressure gradient. The short but engine representative hole length ($L/D = 4$) is constant for all three geometries. The blowing ratio ranges from 0.33 to 2, and the freestream Reynolds number based on the freestream velocity and hole diameter (Re_D) was 8563. Both local values and laterally averaged ones are presented, the latter refers to the averaged value across the central hole. The current results are compared with the experimental results obtained by other researchers, and the effects of variations in injection angle are described.

There is not a single study on film cooling performance of a single round hole at the three streamwise angles for a wide range of blowing ratios with a short hole length. Therefore, the objective of the present study is to provide a consistent set of measurements in terms of effectiveness and heat transfer coefficients [Int. J. Heat Mass Transfer, 2002] obtained systematically on a flat plate, and to deliver a better understanding of film cooling performance, with explanations deduced from the existing knowledge of a single jet in crossflow, before more engine representative conditions are introduced. The present results also serve as a database for future numerical modelling.

1. Introduction

The desire for higher specific thrust in air, land and sea gas turbines renders the need for high temperature-rise combustors, and this, in turn, implies increases in turbine entry temperatures. The turbine blades cannot withstand these temperatures and cooling is required to ensure the required life. It is apparent that internal convective cooling is insufficient to maintain the blade at the required temperatures and, although transpiration may be required in the future, problems associated with the blade strength and the dimensions of the pores remain to be solved. Thus, film cooling is required and usually takes the form of rows of discrete holes along the span of the blades. It is worth noting that the walls of the combustion chamber also have to be cooled and have moved through a similar progression of methods. The gas temperatures are higher in the combustor but the mechanical stresses are less so that special material have been formed for transpiration and supplemented by forms of film cooling. Whatever methods and materials, a major requirement is to ensure that the combustor and blades survive for long periods and with minimum use of cooling air.

The definition of film cooling effectiveness, η is given in the *Nomenclature* section. This effectiveness represents the efficiency of a cooling film, the maximum value of unity is achieved when the adiabatic wall temperature is the same as the coolant temperature. The objective of film cooling is to achieve low heat transfer from the surrounding hot mainstream to the turbine blades, and large effectiveness on the blade surface.

Studies of film cooling effectiveness on streamwise directed holes on a flat plate shown in Fig. 1, have been carried out by researchers such as Eriksen and Goldstein

* Corresponding author. Tel.: +44-20-75947241; fax: +44-20-78238845.

E-mail address: r.botas@ic.ac.uk (R.F. Martinez-Botas).

[1] Currently at ESDU International, London, N1 6UA, England.

0017-9310/03/$ - see front matter
PII: S0017-9310(02)00274-0

Nomenclature

A/D	analogue to digital
AMG	American gage
D	hole diameter
HSI	hue, saturation, intensity
L	hole length
M	blowing ratio ($\rho_2 U_2/\rho_\infty U_\infty$)
Re_D	Reynolds number ($\rho_\infty U_\infty D/\mu_\infty$)
RGB	red, green and blue
SWG	standard gage
T	temperature (K)
TLC	thermographic liquid crystals
U	velocity (m/s)
X	coordinate: streamwise (axial) direction (see Fig. 4)
Y	coordinate: vertical (height-wise) direction (see Fig. 4)
Z	coordinate: lateral direction

Greek symbols

δ	boundary layer thickness
δ^*	displacement thickness $\delta^* = \int_0^\delta \left(1 - \frac{U}{U_\infty}\right) dy$
δ_i	momentum thickness $\delta_i = \int_0^\delta (1 - \frac{U}{U_\infty}) \frac{U}{U_\infty} dy$
η	film cooling effectiveness $\eta = (T_{aw} - T_\infty)/(T_2 - T_\infty)$
ρ	density (kg/m^3)

Subscripts

∞	freestream
2	coolant or secondary injection
aw	adiabatic wall
-	laterally averaged

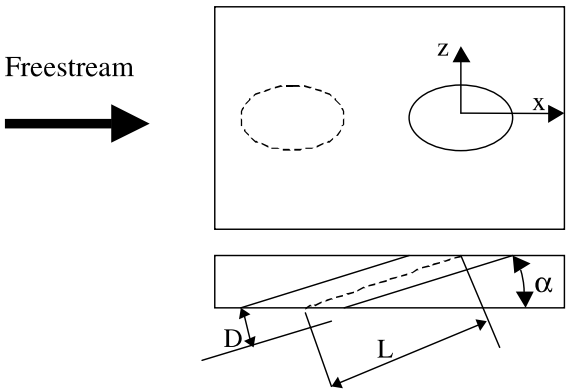

Fig. 1. Hole at an streamwise angle, α.

[2], Goldstein and Yoshida [3], Goldstein et al. [4], Bergeles [5], Brown and Saluja [6], Sinha et al. [7] and Schmidt et al. [8]. The flow pattern of the 30° and 35° jet(s) can take different forms, depending on the blowing ratio, the jet(s) can remain attached, detach and reattach, or lift off completely. From the cited references above, it was suggested for a single jet and a row of jets of a given streamwise inclination, effectiveness near the holes increased with increasing blowing ratio, until a certain value beyond which the jets started to lift off, and the effectiveness decreased, and this ratio is often referred as the optimum blowing ratio. The optimum blowing ratio for a single 30° jet is usually between a blowing ratio of 0.4 and 0.6, and slightly less for a single vertical jet, and the optimum blowing ratio for a row of 30° jets is around 0.5, and relatively less for a row of 60° jets. Comparisons between current results with those of other researchers are discussed in Section 4.

The objectives for the current study are to implement wide band liquid crystal thermography and the steady state heat transfer method to provide two dimensional surface plots of effectiveness for a single round hole at three streamwise angles, with good spatial resolution. An improved knowledge of the surface characteristics of film cooling is achieved by looking at the single hole prior to extending the work to multiple holes where jet-to-jet interactions may be significant, other hole geometries and the effect of a pressure gradient.

2. Characteristics of a jet in a crossflow

2.1. Normal jet

Studies on a single vertical jet in crossflow have been conducted by Keffer and Baines [9], Ramsey and Goldstein [10], Moussa et al. [11], Andreopoulos [12,13], Flack et al. [14], Fric and Roshko [15], Kelso and Smits [16], Kelso et al. [17] and Sivadas et al. [18]. Margason [19] described the ring (shear-layer) vortices on the circumference of a vertical jet, the near-wall horseshoe vortex, the dominant longitudinal counter-rotating vortex pair and the wake vortices (Fig. 2). Some findings are described in the following paragraphs, and they were with velocity ratios (U_2/U_∞) ranging from 2 to 10, which are larger than those in film cooling applications, as their research was motivated by vertical/short take-off and landing aircraft.

Researchers [11,13,20] suggested that the counter-rotating vortex pair is formed by the shear-layer which emanates from the hole, and Bergeles et al. [21] and Crabb et al. [22] suggested that the counter-rotating pair

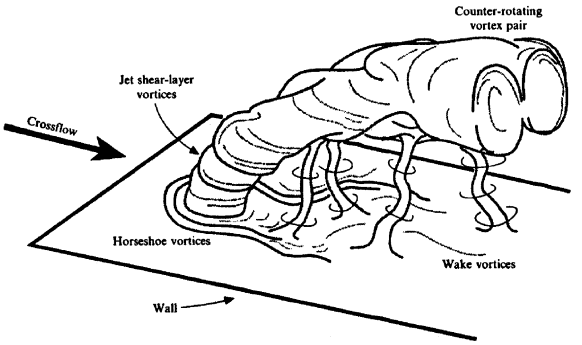

Fig. 2. Jet in crossflow, Fric and Roshko [15].

may be initiated within the pipe itself. The jet is moved away from the wall by this vortex pair, and the strength of this counter-rotating motion amplifies with increasing blowing ratio. Induction lift is generated when the two counter-rotating vortices are in close proximity of each other, and these vortices are known to have a detrimental effect on film cooling performance [23].

The wake vortices which resemble the von Karman vortex street are shed from the vorticity which originates in the boundary layer of the crossflow wall. The upright vortices in the wake of the jet start from the wall boundary layer, and the other end is entrained by the jet [15].

Bergeles et al. [21] found that the velocity profile across the exit plane of a single vertical jet can be non-uniform and more so with low blowing ratios, and this was independently established by Crabb et al. [22] who also examined the kidney vortex as the jet turned and moved downstream. Andreopoulos and Rodi [20] found that the crossflow acted like a partial cover over the exit with a blowing ratio of 0.5, and caused the flow inside the hole to exit near the downstream side with greater velocity than the freestream.

Bergeles [5] and Andreopoulos and Rodi [20] found a region of reverse flow close to the wall behind the vertical round jet, into which the crossflow fluid entered, travelled upstream and was lifted upwards by the jet fluid and transported downstream. Bergeles [5] reported that the reverse flow region extended approximately two diameters downstream of the hole and one diameter wide with a vertical jet at a blowing ratio of 0.24.

Crabb et al. [22] found that a recirculation region began at y/D of 0.75 and x/D of 0.75 in the centreplane and extended for a length of half a diameter, and attributed this to the combined blockage of the jet and the vortex structure. The recirculation zone developed to one diameter wide and 1.5 diameters long by y/D of

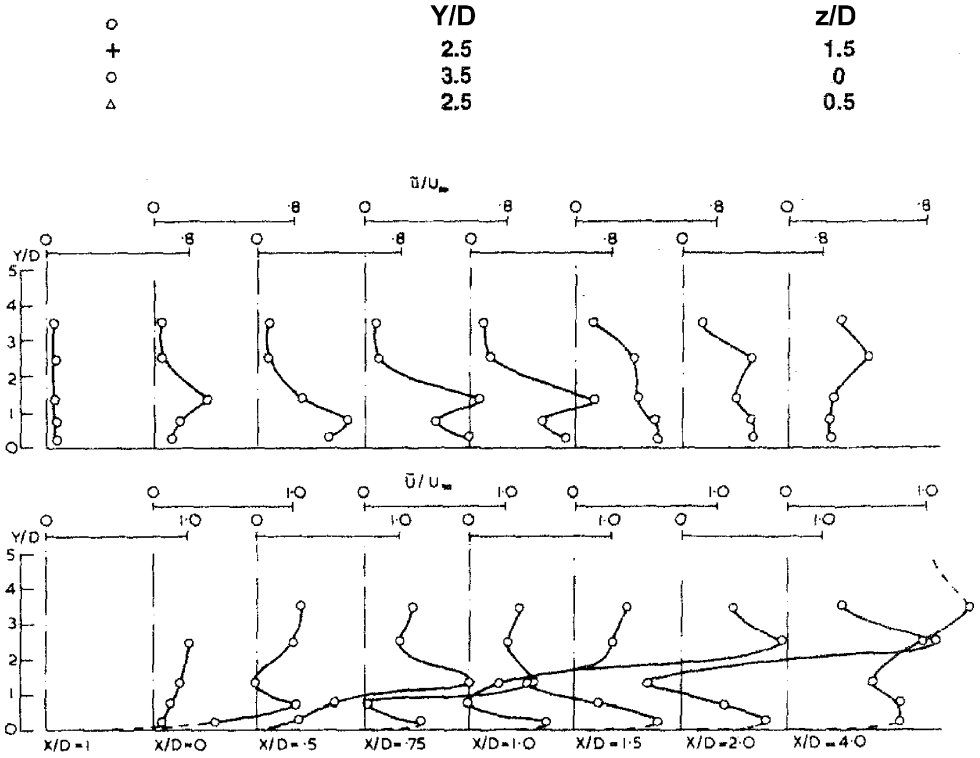

Fig. 3. Centreplane mean velocity and normal stress profiles, Crabb et al. [22].

1.35, extending to nearly x/D of 3 where the vortex centre began to move outwards, and the jet was turned into the crossflow direction by y/D of 2.5. Crabb et al. [22] showed that a peak velocity began on the centre-plane at x/D of 0 (Fig. 3) and continued at x/D of 0.5 and 0.75, and was destroyed by x/D of unity at which the recirculation zone commenced, and became strong at x/D of 1.5.

2.2. Inclined jet

Although inclined jets are widely used in film cooling applications, there have been few investigations of flow structure. Lee et al. [24] confirmed the existence of the counter-rotating vortex pair downstream of a 30° jet. Pietzryk et al. [25] found a small reverse flow region behind the jet and documented the existence of shear layers in the flowfield, such as the crossflow above the jet, the jet itself, and the wake region, and (for higher blowing ratios) the entrained crossflow fluid beneath a 35° jet. Bergeles [5] found a small reverse flow region of less than two diameters long and less than one diameter wide downstream of a single 35° jet at a blowing ratio of 0.24.

Walters and Leylek [23] reported a reverse flow region that comprised of slow moving fluid in the crossflow boundary layer beneath the 35° jet from a pipe with a length-to-diameter ratio of 3.5 and a saddle point where the crossflow fluid moving toward the centreline from either side met. They also verified that the non-uniform distribution of jet profile with the single vertical jet obtained by researchers [5,20,22,26], was present with the 35° jet, and suggested that its extent depended on the length-to-diameter ratio of the pipe which transported the jet fluid, blowing ratio and geometry. The length-to-diameter ratio of the pipe used by Bergeles [5], Andreopoulos and Rodi [20] and Pietrzyk et al. [26] was 50, 12 and 3.5 respectively. The fluid in the film hole shifted towards the trailing edge at low blowing ratios, and was pushed towards the leading edge at large blowing ratios. The effects of the separated flow inside the cooling hole had less time to attenuate as the length-to-diameter ratio decreased, and exerted more influence on the jet exit conditions.

3. Experimental apparatus and procedure

3.1. Liquid crystal thermography

Baughn [27] reviewed methods of involving narrow band crystals and wide band liquid crystals for measurements of local heat transfer coefficients with both the steady state and transient state techniques. Most of the work used crystals with a narrow band, such as by [28–32]. Multiple mixtures of liquid crystals have been used to obtain more than one isothermal line per image, such as Van Treuren et al. [33] who applied three encapsulated liquid crystals and traced the intensity-time history for an array of impinging jets. Babinsky and Edwards [34] used very wide band crystals of temperature ranging from 27.6°C (red) to 41.5°C (blue) with the transient heat transfer method in a hypersonic flow.

In the present study, wide band crystals and the steady state heat transfer method are implemented. The details of this technique are provided in Yuen [35]. The encapsulated liquid crystal used in current study supplied by Thermax Ltd. [2] offers a bandwidth of 10 °C. The liquid crystal itself is colourless, therefore in order to enhance its colour displayed, the test surface was sprayed black with an oil-based black ink compatible with the liquid crystals.

3.2. Test facility

The test rig has a modular design, and is presented in Fig. 4. The details of the test facility are given in Yuen [35]. The test section consists of a 40 mm long knife bleed, which ensures precise control of the boundary layer origin, and an injection plate, which is interchangeable with other plates containing different cooling hole geometries. Three injection plates were made of Perspex, and each plate contained two rows of nine holes of the same geometry and these were cylindrical holes with streamwise inclinations of 30°, 60° and 90°. For the single hole tests presented in this paper, the centre hole in the downstream row was used whilst the other holes were covered with thin tape. The holes were positioned as close as possible to the downstream edge of the injection plate, such that the trailing edge of the holes was 6 mm from the downstream edge of test plate, which was desirable from the view point of measurements.

The composite test plate is 360 mm wide × 1000 mm long × 163 mm thick, and is well insulated by a 10 mm thick Tufnol sheet which has good thermal resistance and mechanical strength and a 150 mm thick Styrofoam block, to approximate a near-adiabatic wall (Fig. 5). Details of the test plate are given in the companion paper [1] which presents the heat transfer measurements and Yuen [35]. It has the capacity to produce a constant heat flux for heat transfer measurements, but it is not heated for the measurements of effectiveness. Ten T-type (copper–constantan, AMG 36, SWG 39-40) thermocouples were installed under the. uppermost layer (stainless steel sheet).

[2] Thermax (Thermographic Measurements Ltd.), Bank House, Neston Road, Burton, South Wirral L64 5TA, England.

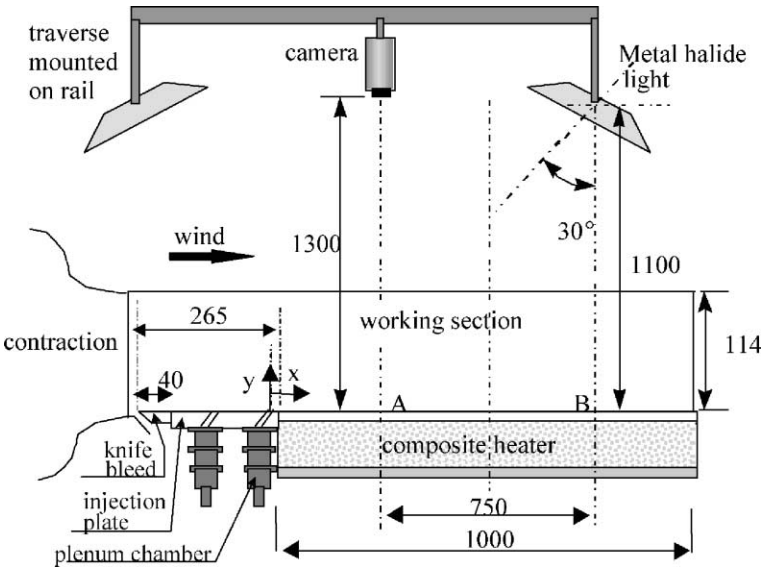

Fig. 4. Experimental set-up.

3.3. Image processing and calibration

The imaging system used comprised of a colour JVC CCD camera, two light sources, and a 24-bit frame grabber installed in a computer. The test section was contained in a spacious tent made of anti-flammable black cloth to eliminate variations in illumination, such as the time of day, and was sufficiently large for air circulation.

The temperature and hue calibration for the liquid crystals was performed on the actual test surface, without the crossflow or injectant. The electrical power supplied to the test surface was increased incrementally until the entire spectrum of colour play was displayed. For each setting of electrical power input, 25 images were captured at 25 frames/s, once surface temperature and colour had stabilised, typically after 45 min of running, the corresponding temperatures from the thermocouples were recorded by two A/D modules which were calibrated with a precise voltage source and utility software with cold junction compensation (CJC) incorporated. The accuracy of the calibrated thermocouples are ± 0.5°C. The images captured were then converted from the RGB to HSI format. In the current investigation, 1968 frames were used in each calibration. The camera settings, light source, distance, and angle were kept the same both for calibration and the actual experiments. The calibration procedure was repeated three times during the whole series of test cases, the results showed no calibration drift.

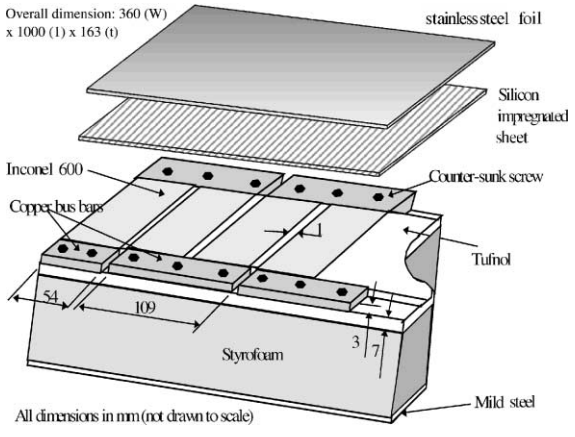

Fig. 5. Test plate with a constant heat flux.

3.4. Data reduction

The test plate occupies 1524×1044 pixels with 1 pixel approximately equals to 0.7 mm on the image. It is clear that if every individual pixel is represented in post-processing, there will be an overflow of information. A test was performed to compare the performance with pixel-to-pixel value and a matrix of cells made up of 3×3 pixels. Similar methods were adopted by Farina et al. [36] in image post-processing, and Babinsky and Edwards [34] in the calibration phase. Both sets of results collapsed on the same curve for different runs, which indicated that localised features emerging from the pixel-to-pixel post-processing were repeated accurately with the matrix of 254 (stream-wise direction) by 174 (cross-wise direction) cells.

Table 1
Test cases

Configuration	Streamwise angles	Hole length (L/D)	Blowing ratio (M)	Re_D
Single hole	30°, 60° and 90°	4	0.33, 0.5, 0.67, 1.0, 1.33, 1.67 and 2.0	8563

3.5. Experimental uncertainty

Uncertainties are evaluated by the method of Kline and McClintock [37]. Corrections are applied to consider heat loss through thermocouple leads using the method proposed by Schneider [38]. The uncertainty in η is approximately $\pm 9\%$ respectively.

3.6. Operating conditions

Freestream velocity was maintained at 13 m/s, the corresponding Reynolds number based on the hole diameter and freestream velocity, Re_D, was 8563. The freestream temperature was 20 °C and the turbulence intensity was 2.7%, and the injectant-to-freestream blowing ratio varied from 0.33 to 2. The effectiveness tests were carried out with the test plate unheated to approximate an adiabatic surface, and the injectant was heated by an in-line heater to 40 °C ($\rho_2/\rho_\infty = 0.92$). The temperature differences between the freestream and the injectant were small enough to neglect the property variations, so that the results can be applied to film cooling problems [39]. The jet temperature was measured by a T-type thermocouple at the hole exit and in the plenum chamber. The difference between these temperatures was approximately 0.1 °C. The injectant temperature refers to that at the hole exit. The test cases investigated in the current study are listed in Table 1.

The boundary layer thickness grows from approximately $\delta/D = 0.1$ at $x/D = -24.8$ (see Fig. 4 for the location of the measuring axis) to approximately $\delta/D = 1.0$ at the injection plane ($x/D = 0$). The displacement thickness (δ^*/D) and momentum thickness (δ_i/D) are 0.15 and 0.11 respectively at the plane of injection.

4. Results

In the results presented here, the axial range is classified into four regimes for clarity: the immediate region for $x/D \leqslant 3$, the near field for $3 \leqslant x/D \leqslant 7$, the intermediate region for $7 \leqslant x/D \leqslant 26$, and the far downstream region for $x/D \geqslant 26$.

4.1. Hole with 30° injection

The distribution of adiabatic effectiveness for a single 30° cooling hole is shown in the form of two-dimensional surface contours with blowing ratios in the range from 0.33 to 1.67 in Fig. 6. The direction of crossflow is from left to right, the origin of the axial distance, x/D, and lateral distance, z/D, commence from the centre of the cooling hole, as shown in Figs. 1 and 4, and the chosen interval of η is 0.05. The symmetry was excellent in the upstream region, and the asymmetric scatter far downstream, where $0 \leqslant \eta \leqslant 0.1$, fell within the uncertainty band discussed at the end of the paper. The effectiveness contracted length-wise, and laterally as the blowing ratio increased from 0.33 to 1.67. The total lateral spread was approximately three to four diameters in width, in accord with that found by Goldstein et al. [40]. The axial distance travelled by the jet from the point of injection increased in distance from the test surface, and the effectiveness was expected to decrease with downstream distance, as observed. The centreline effectiveness and the lateral spread in Fig. 6 decreased with increasing blowing ratio due to the penetration of the jet into the mainstream for blowing ratios greater than 0.5.

The more effective region (with $\eta > 0.2$) did not extend beyond x/D of 13, with the maximum effectiveness of approximately 0.4 in the immediate region. This region increased marginally as the blowing ratio was increased from 0.33 to 0.5, and then decreased with further increase in blowing ratio. The same experiments were repeated with a lower Re_D of 4800, and the distribution was found to be similar to that with Re_D of 8563.

Fig. 7(a)–(f) shows the distribution of effectiveness for different lateral locations and blowing ratios in the form of a scatter plot. The symmetry demonstrated in Fig. 6 led to the presentation of results for the positive values of z/D only. The general trend with all the blowing ratios tested was for the centreline effectiveness to decay rapidly with increasing axial location for the first ten diameters, and then gradually to tend to zero. The effectiveness decreased monotonically with increasing axial distance for lateral positions, on or near the centreline of the jet for a given blowing ratio. Eriksen [41] found that the effectiveness initially increased at positions away from the centreline, before decreasing as the jet mixed with the mainstream, and this is not the case here for several reasons. First, Eriksen's measurements started from approximately x/D of 5, where the near wake information may not have been captured. Second, the review of jets in crossflow, showed that the non-dimensional hole length greatly affected the emerging jet profile, and it is reasonable to deduce from that, that the mechanism between the crossflow and jet in the current investigation is different to Eriksen's study since he used a long injection tube ($L/D \approx 62$) with a

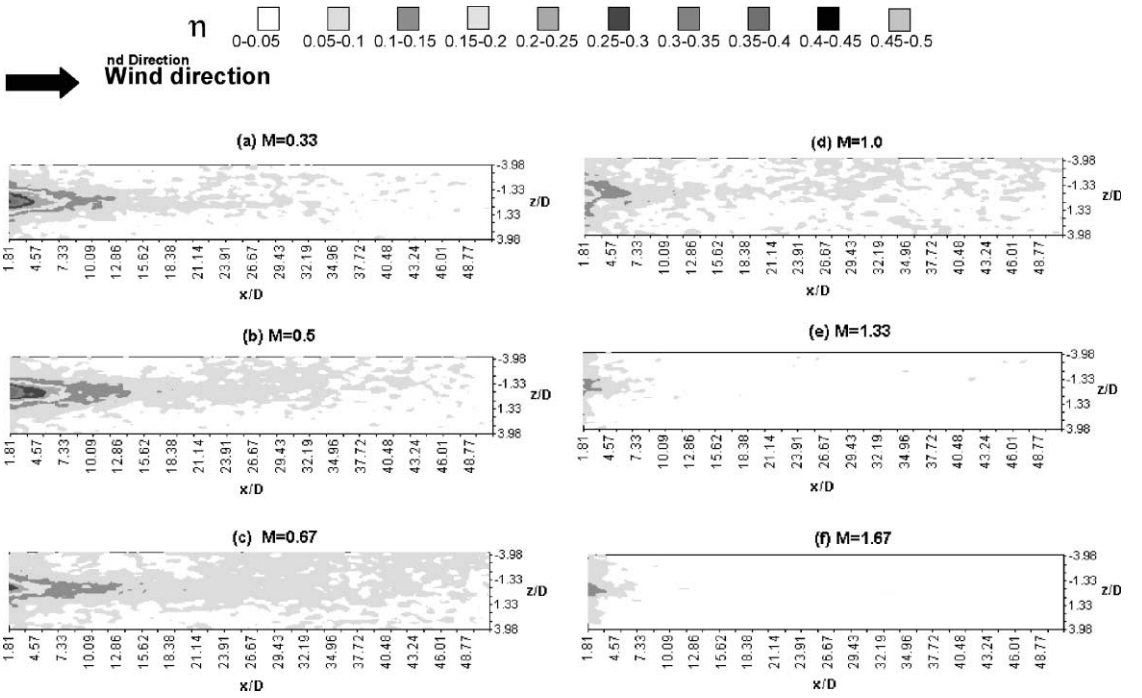

Fig. 6. Film cooling effectiveness for a single 30° hole.

fully developed pipe flow. The initial relatively low effectiveness of Eriksen [41] at lateral positions implies that the effect of the coolant was absent for some distance downstream from the point of injection, in part because the lateral positions were beyond the edge of the jet where jet spreading was relatively small. As the jet progressed downstream, it spread to provide increased effectiveness, before gradually levelling and ultimately decreasing. The discrepancies between his findings and those reported here suggest that his jet spreading was less than that observed here.

The centreline effectiveness was larger than that at other lateral positions shown for axial locations less than x/D of 10, the distance required by the jet to mix with the mainstream to achieve a lateral quasi-equilibrium for all blowing ratios tested. Fig. 7 shows that film cooling was not as effective at high blowing ratios as at low ratios, which is in accord with Bergeles [5], Goldstein et al. [40,42] and Eriksen [41].

Close examination of the results at a blowing ratio of 0.33 (Fig. 7(a)) reveals a small discontinuity, or plateau, close to x/D of 6 and z/D of 0 and 0.5, and this became more apparent at blowing ratios of 0.5 and 0.67, and may represent the positions at which re-attachment began. Fig. 7(b) shows that the maximum effectiveness decreased from 0.45 at a blowing ratio of 0.33 to 0.4 at a blowing ratio of 0.5, and the off-centre values of effectiveness at a blowing ratio of 0.67 were similar to those at a blowing ratio of 0.33, indicating that the lateral spread of the jet ceased to increase, as a result of the smaller velocity gradient between the jet and the adjacent fluid.

Fig. 8 assembles the distributions of centreline effectiveness for all blowing ratios, including the results of Goldstein et al. [40], who studied film cooling with a single 35° streamwise inclined long pipe, ($L/D \approx 42.6$) and Re_D of 0.44×10^5. There is good qualitative agreement with the current 30° hole, but their values were consistently higher. The common qualitative trends include the small peak in effectiveness near the hole indicating jet re-attachment, as observed by Sinha et al. [7] who studied adiabatic effectiveness with a single row of 35° holes and found the peak value between x/D of 3 and 6 for higher blowing ratios. The overall decrease in effectiveness with increasing downstream distance and increased jet mixing is also a common feature, as is better film cooling at smaller blowing ratios.

The difference in the magnitudes of effectiveness between the current results and those of Goldstein et al. [40] are caused by a combination of factors including the large difference in Re_D, the boundary layer thickness in the plane of injection and the length-to-diameter ratio (L/D), and these are discussed in turn in the following paragraphs.

Eriksen and Goldstein [2] showed that the effectiveness increased with Re_D, though by a small amount. This increase is not consistent with the increased interaction expected between the jet and the surrounding fluid,

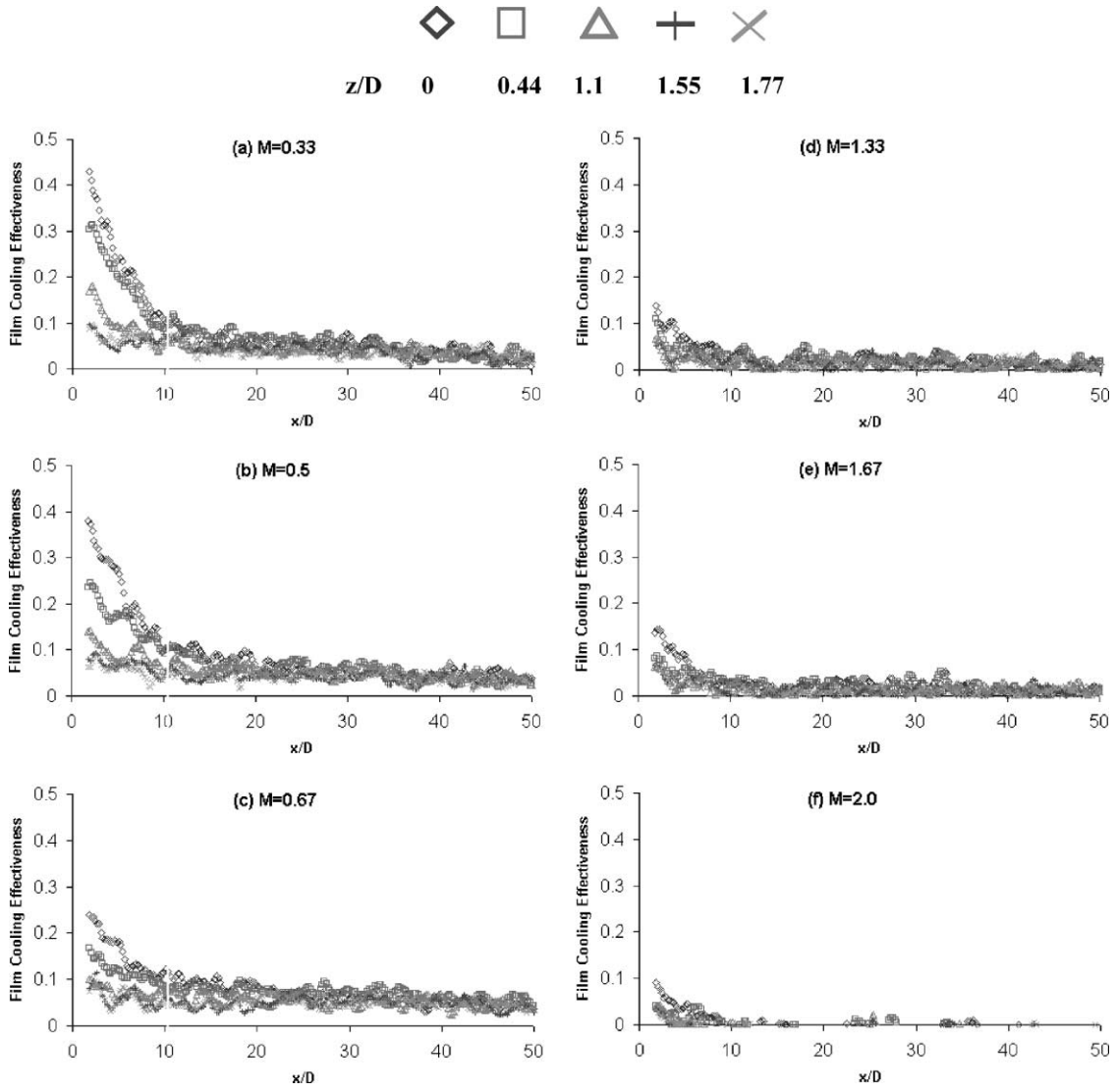

Fig. 7. Lateral distributions of effectiveness with a single 30° hole.

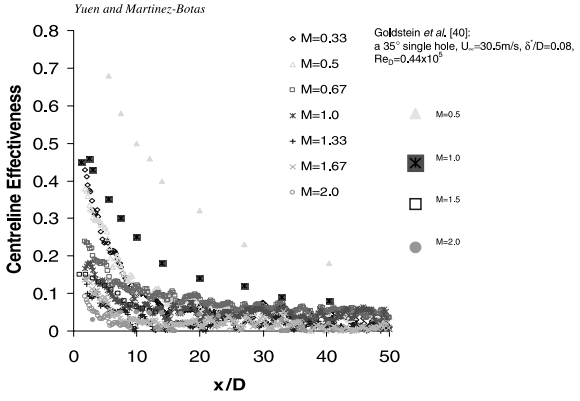

Fig. 8. Variations of centreline effectiveness for a 30° hole.

which should result in lower effectiveness. However, the boundary layer thickness is also dependent of the Reynolds number, and effectiveness decreased as the thickness of boundary layer increased. The displacement thickness in the injection plane of Goldstein et al. [40] was approximately half (δ^* of 0.08) that in the present study (δ^* of 0.15).

Bergeles [5] considered the effects of displacement thickness on effectiveness, and concluded that it was important for blowing ratios at which the jet was about to lift off. He also found that the blowing ratio at which the maximum effectiveness occurred depended on the boundary layer thickness. With δ^*/D of 0.095 and δ^*/D of 0.078 at the injection plane, the largest effectiveness occurred with blowing ratios of 0.5 and 0.75 respec-

tively. Kadotani and Goldstein [43] showed that the largest effectiveness was found with a blowing ratio of 0.35 when δ^*/D in the plane of injection was 0.175. The δ^*/D in the current study was approximately 0.15, and the maximum effectiveness was achieved with blowing ratios less than 0.5 both close to and away from the hole. Goldstein et al. [40] found that doubling the displacement thickness of the main flow boundary layer caused a decrease of the effectiveness by 30% with a blowing ratio of 0.5.

The length-to-diameter ratio, L/D, used by Goldstein et al. [40] was large, and delivered fully developed pipe flow at the hole exit, compared to the very short, but engine-representative cooling hole (L/D of 4) used here. Sinha et al. [7] suggested that a small length-to-diameter ratio would lead to larger effective injection angles, which would, in turn, result in jet lift-off at a smaller momentum-flux ratio ($\rho_2 U_2^2/\rho_\infty U_\infty^2$).

Fig. 9 summarises the effects of blowing ratio on effectiveness at certain axial locations respectively. The results of Goldstein et al. [40] with a Re_D and δ^*/D of 88,000 and 0.08 respectively are included in Fig. 9, and may be compared to the current results with Re_D of 8563 and δ^*/D of 0.15. The maximum effectiveness was achieved in the immediate region with blowing ratios less than 0.5 and with a blowing ratio of 0.5 for locations downstream of the immediate region, similar to those of Goldstein et al. [40]. The consistently lower effectiveness displayed in the current study is related to the difference in Reynolds number (almost ten fold), hole length-to-diameter ratio (slightly more than ten fold) and the boundary layer displacement thickness (approximately two fold), as discussed previously.

The variation of laterally averaged film cooling effectiveness with blowing ratio is illustrated in Fig. 10, which includes the results of Brown and Saluja [6] who measured a row of holes with a pitch-to-diameter ratio of 5.33, a length-to-diameter ratio of 14.7, and a turbulence intensity of 1.7% and 8%. Their maximum effectiveness was achieved with a blowing ratio of 0.3 and x/D of 5, which may be compared to the peak effectiveness found here with a blowing ratio of 0.5 and at a similar axial location. Fig. 10 also shows that the blowing ratio at which the maximum effectiveness occurred, increased with downstream distance, since more momentum was required to transport the jet further.

4.2. Holes with 60° and 90° injection

The contour plots in Fig. 11 for a single 60° hole with blowing ratios ranging from 0.33 to 1.67, show that the largest effectiveness was less than that with the 30° single hole, since the vertical velocity component was greater with a steeper hole. The effectiveness was unchanged by the injection angle for blowing ratios less than unity, but the effect of the angle became more apparent as the blowing ratio increased beyond unity.

The effectiveness values for a single 90° hole with blowing ratios in the range from 0.33 to 1.67 in Fig. 12 are similar to those with a single 60° hole and blowing ratios less than 0.67, and smaller than those with the 60° hole for blowing ratios greater than 0.67. The protected region is also shorter. In general, the 90° jet did not reach the wall for intermediate and large blowing ratios ($M \geqslant 0.67$). The centreline effectiveness values for the single holes of Figs. 6, 11 and 12, were larger than those

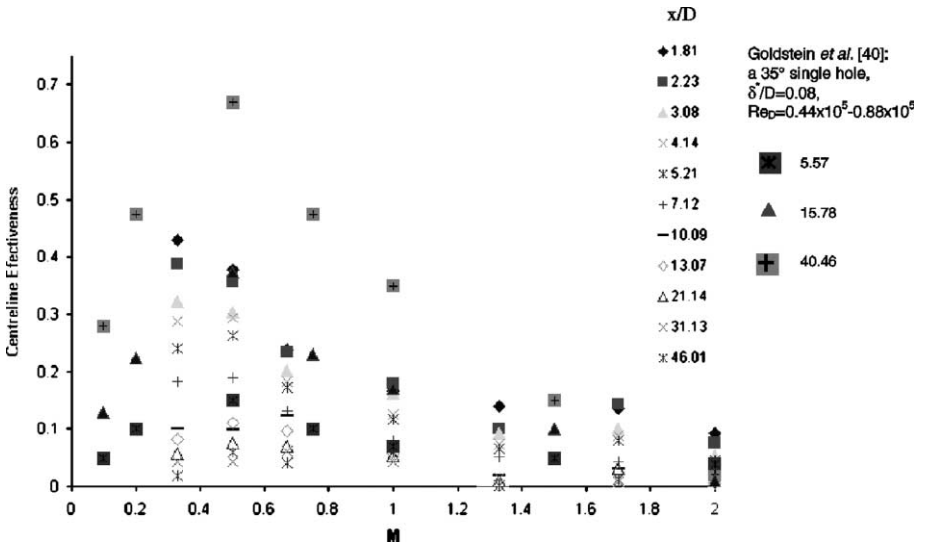

Fig. 9. Variations of centreline effectiveness with blowing ratio for a 30° hole.

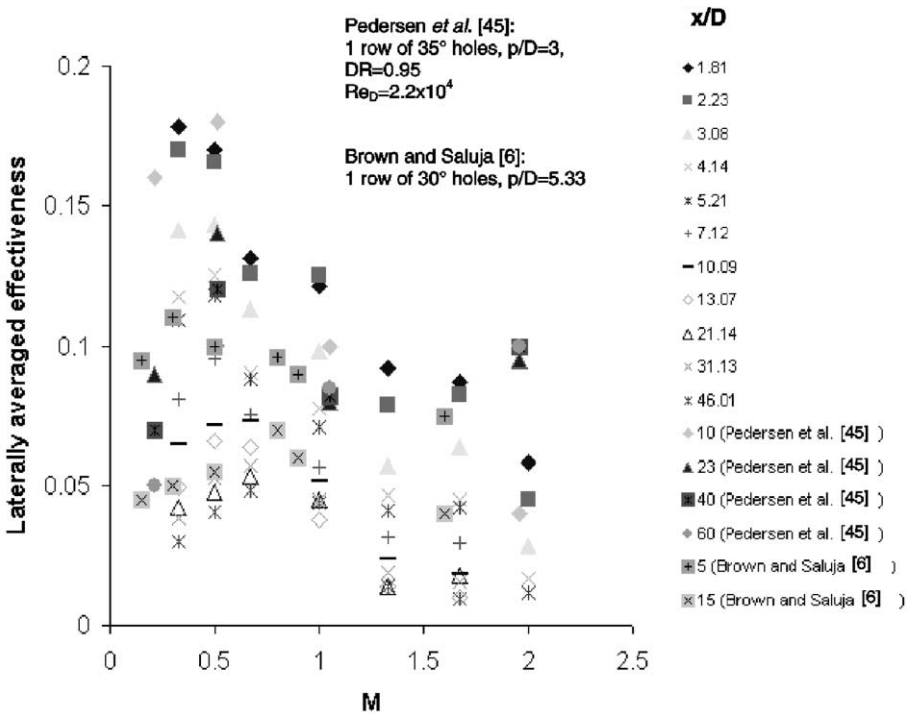

Fig. 10. Optimum blowing ratio for laterally averaged effectiveness for a single 30° hole.

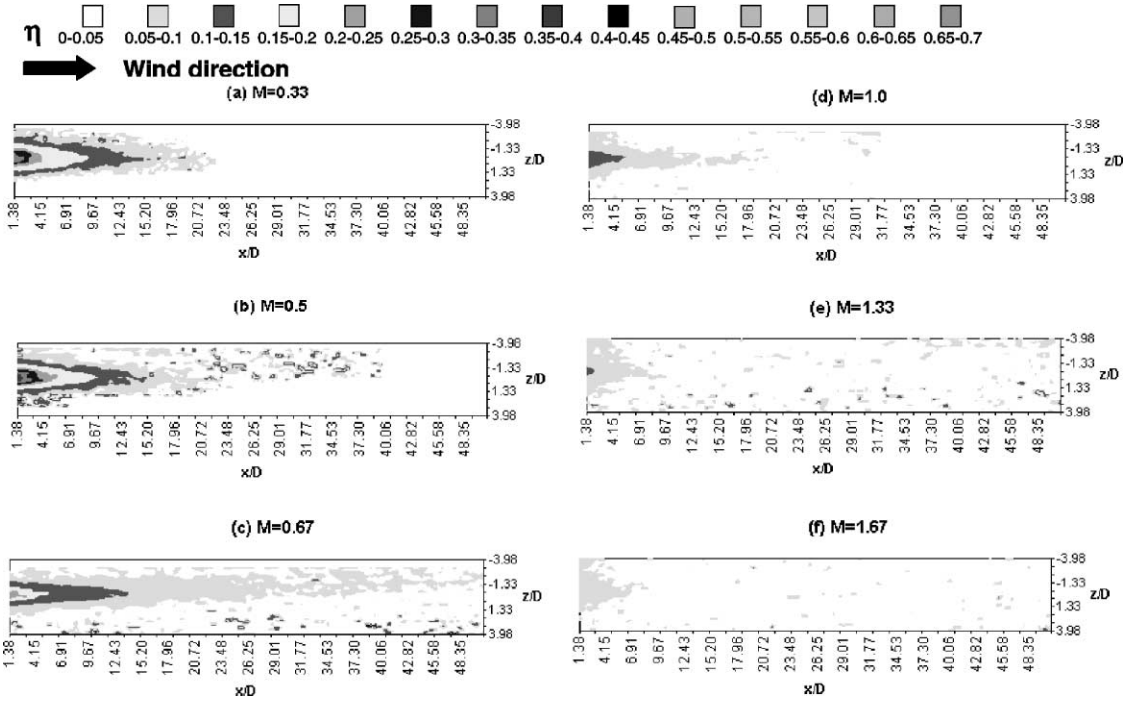

Fig. 11. Film cooling effectiveness for a single 60° hole.

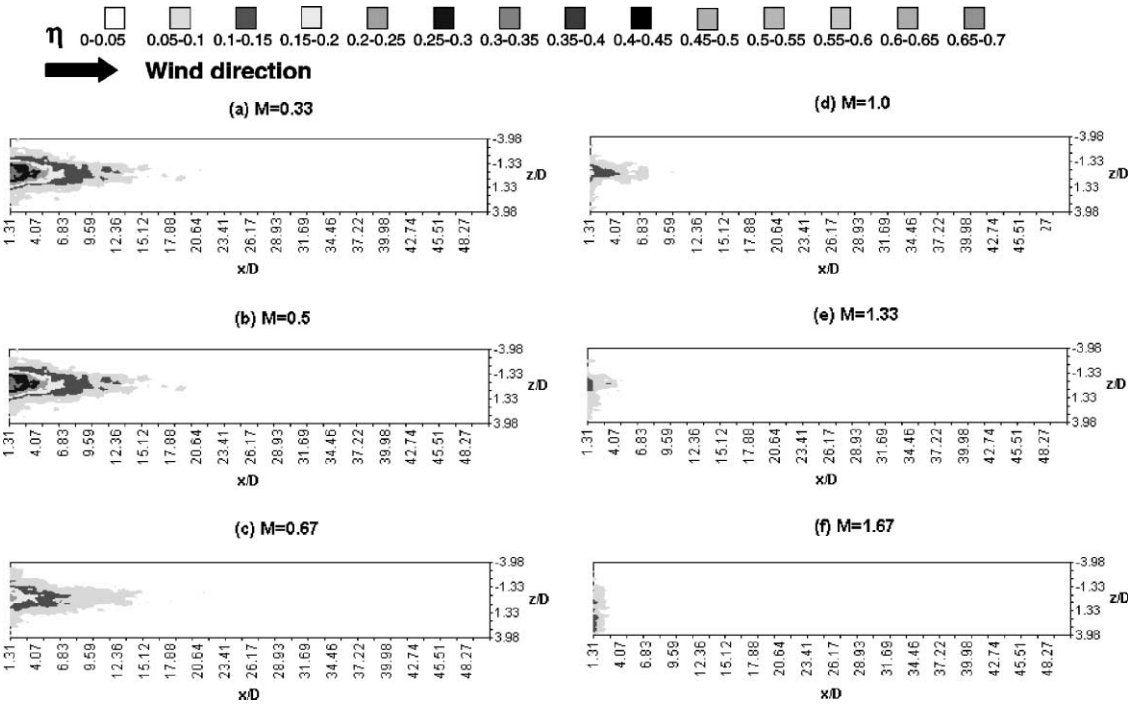

Fig. 12. Film cooling effectiveness for a single 90° hole.

at finite radii for axial locations upstream of x/D of 40, 17.5, and 15.5 for the 30°, 60° and 90° angles respectively with a blowing ratio of 0.5, which implies that the rate of spread was the most rapid for normal jet, and slowest for the 30° jet. A more detailed comparison of the three streamwise angles is given in the next section.

4.3. Effects of jet angle

Fig. 13(a)–(f) allows comparison of the variations of centreline effectiveness for the three angles. In general, the effectiveness achieved with the 30° jet ($\eta_{30°}$) was larger than that obtained with the 60° jet ($\eta_{60°}$), and the value with the 60° jet ($\eta_{60°}$) was higher than that with the 90° jet ($\eta_{90°}$).

The maximum effectiveness achieved by the 30° jet in the immediate region with a blowing ratio of 0.33 (Fig. 13(a)) was approximately 20% higher than that by the steeper (60° and 90°) jets. However in the near field, $\eta_{30°} > \eta_{90°} > \eta_{60°}$; and in the intermediate region, $\eta_{60°} > \eta_{30°} > \eta_{90°}$; and, finally, $\eta_{30°} > \eta_{60°} > \eta_{90°}$ far downstream. The 30° jet remained closest to the wall, the 60° jet was vertically further from the wall, and the 90° jet was the furthest, therefore, the descending order of $\eta_{30°} > \eta_{60°} > \eta_{90°}$ was found in the immediate region. In the near field, the shallowest angle provided the best protection with its lowest trajectory, but the 60° jet was expected to provide better effectiveness than the 90° jet, since it had less vertical momentum than the 90° jet, but this was not the case. The 90° jet had the greatest vertical momentum when it emerged from the hole, and should penetrate furthest into the crossflow to give the lowest effectiveness.

In order to understand these features and trend reversals, it is essential to recall from the review in the literature survey presented earlier that the velocity distribution across the hole exit may be skewed towards the trailing edge of the hole with low blowing ratios and thin boundary layer, in other words a maximum velocity occurs in the downstream half of the hole, and it is larger than that of a turbulent jet for the same mass flow. This non-uniform velocity distribution of the exiting jet is referred to as jetting hereafter, and it depends on the hole geometry and the blowing ratio as suggested earlier. The amount of fluid in the surrounding boundary layer which is re-entrained into the jet wake varied with the extent of jetting. Brundage et al. [44] suggested that the pressure build up within a single hole at 35° and 90° with length-to-diameter ratios of 1.16 and 2.91. The projection of an inclined hole onto the horizontal surface changed accordingly, the major axis is 2 diameters long with the 30° hole, 1.15 diameters in length with the 60° hole, and 1 diameter long with the normal hole. It is probable that the bias of the exiting jet fluid towards the lee-side of the hole varied with streamwise angles. Furthermore, the 90° jet caused more disturbance to the flow upstream of the hole, in contrast to the 30° jet [5], so that the combination of jetting in the shortest projected

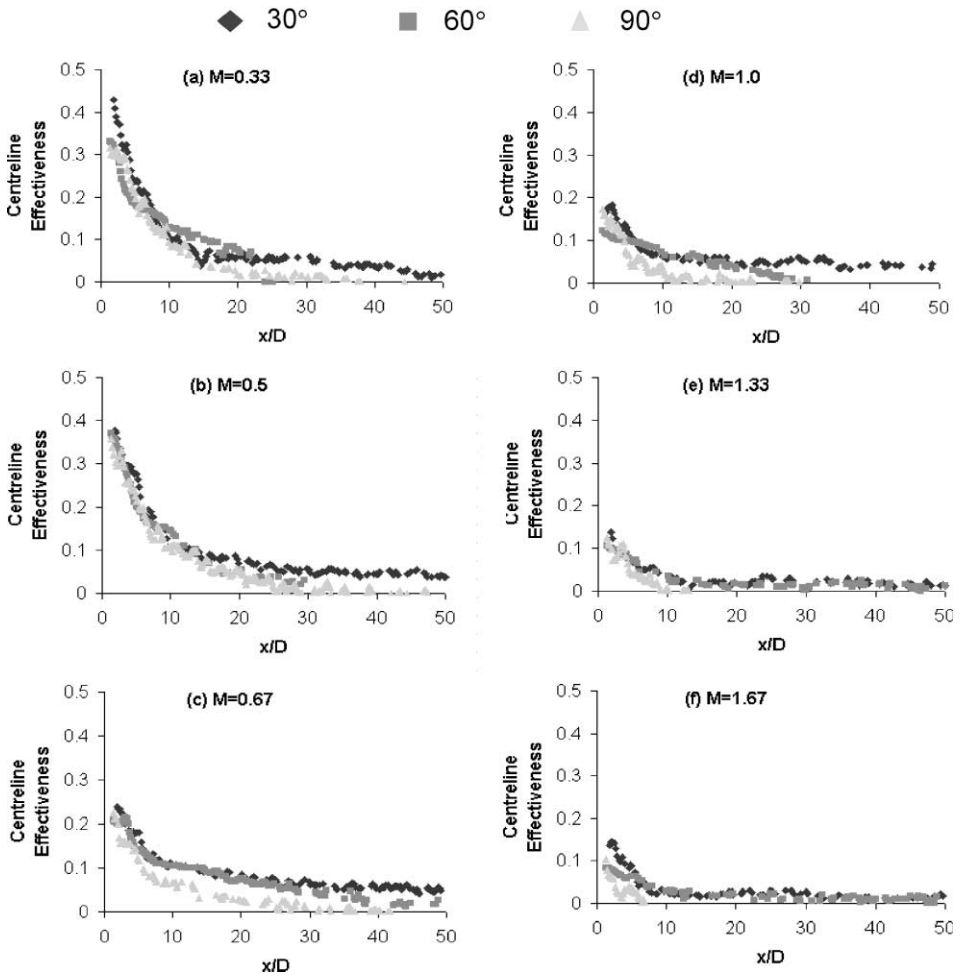

Fig. 13. Effects of streamwise angle on centreline effectiveness for a single hole.

exit and the pressure gradient across the normal hole may be responsible for the trend of $\eta_{30^\circ} > \eta_{90^\circ} > \eta_{60^\circ}$ in the near field. It is probable that the jet fluid was pulled into its own wake by the accelerating freestream around the 90° jet and entrained the lower momentum jet fluid [22]. This mechanism existed with the 60° angle, but its strength was weak, because of a weaker blockage and a smaller pressure gradient.

Moving downstream to the intermediate region with a blowing ratio of 0.33 in Fig. 13(a), the 30° jet has already been transported by the dominant counter-rotating vortex pair downstream, and the 90° has penetrated into the freestream, thus $\eta_{60^\circ} > \eta_{30^\circ} > \eta_{90}$. The trend returned to its original order, $\eta_{30^\circ} > \eta_{60^\circ} > \eta_{90^\circ}$ far downstream. The effectiveness was similar with the three angles over the first ten and five diameters with a blowing ratio of 0.5 (Fig. 13(b)) and 0.67 (Fig. 13(c)) respectively, which implies that the handicap in axial momentum with the steeper angles of 60° and 90° was compensated by the shear at the periphery which brought some of the warmer jets towards the wall. Andreopoulos and Rodi [20] reported that the boundary layer fluid was re-entrained into the upstream part of a 90° jet, and as a result, it was possible that the vortex transported the warmer fluid in the jet downstream, which then compensated for the axial momentum deficit with the steeper angles. The trend of $\eta_{30^\circ} > \eta_{90^\circ} > \eta_{60^\circ}$ was found with a blowing ratio of unity in Fig. 13(d) in the near field, which is similar to the trend already encountered with the blowing ratio of 0.33 at the same location, for the explanations already given. Further increase in the blowing ratios to 1.33 and 1.67 in Fig. 13(e) and (f) respectively provoked little change in effectiveness values for all three angles, for they have all dispersed into the freestream, and had little effect on the wall.

The distributions of the laterally averaged effectiveness for the three angles are presented in Fig. 14(a)–(f)

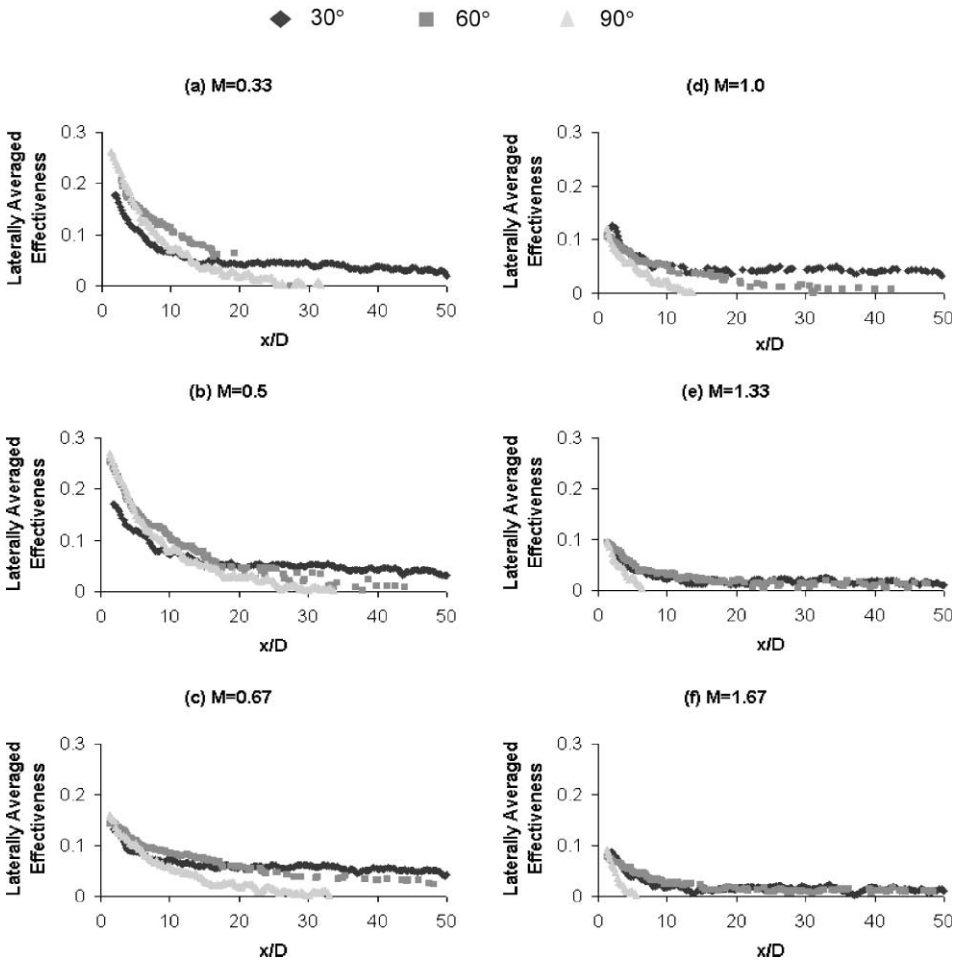

Fig. 14. Effects of streamwise angle on laterally averaged effectiveness for a single hole.

and the expected and "contradictory" trends found in the centreline effectiveness are repeated here. The laterally averaged effectiveness and the corresponding rate of decay decreased with increasing x/D, and they are both lower than those on the centreline due to jet spreading.

5. Conclusions

1. For a single 30° hole, the more effective region (with $\eta > 0.2$) did not extend beyond x/D of 13. In the immediate region, the maximum effectiveness was achieved with blowing ratios less than 0.5; whilst for regions downstream of the immediate region, the maximum value was achieved at the blowing ratio of 0.5 and the momentum flux ratio of 0.3, as more momentum was required to transport the jet further. Film cooling at high blowing ratios was not as effective as at low ratios.
2. The level of effectiveness in the present investigation is consistently lower than that in the work by Goldstein et al. [42], but the qualitative trends are similar. The difference in their values and the current results could be caused by a combination of factors including the large difference in Reynolds number, the boundary layer displacement thickness in the plane of injection, and the length-to-diameter ratio. A long hole delivers a fully developed pipe flow at the hole exit, and a short hole leads to larger effective injection angles which would, in turn, result in jet lift-off at a smaller blowing ratio. The difference in effectiveness value suggests that jet spreading in their study was less than that observed here.
3. The maximum effectiveness achieved by the 30° hole in the immediate region with a blowing ratio of 0.33 was approximately 20% higher than that by the steeper (60° and 90°) holes. However in the near field, $\eta_{30^\circ} > \eta_{90^\circ} > \eta_{60^\circ}$; and in the intermediate

region, $\eta_{60°} > \eta_{30°} > \eta_{90°}$; and, finally, $\eta_{30°} > \eta_{60°} > \eta_{90°}$ far downstream.

4. The descending order of $\eta_{30°} > \eta_{60°} > \eta_{90°}$ was found close to the hole because the 30° jet remained closest to the wall, the 60° jet was vertically further from the wall, and the 90° jet was the furthest. Moving downstream to the intermediate region with a blowing ratio of 0.33, the 30° jet has already been transported by the dominant counter-rotating vortex pair downstream, and the 90° jet has penetrated into the free-stream, thus $\eta_{60°} > \eta_{30°} > \eta_{90°}$. Far downstream, the trend returned to its original expected order, $\eta_{30°} > \eta_{60°} > \eta_{90°}$.
5. The effectiveness provided by all three angles were similar for blowing ratios of 0.5 and 0.67, within the first ten diameters and five diameters respectively, which implies that the handicap in axial momentum for the steeper angles of 60° and 90° was compensated by the shear at the periphery bringing some of the warmer jets towards the wall. The "contradictory" trends found in the centreline effectiveness were repeated in the laterally averaged effectiveness.

Acknowledgements

The authors would like to thank Alstom Power Ltd., particularly Prof. J. Hannis, Dr. J. Turner, Dr. Gan for supporting the present work, and Thermax Ltd. for providing the liquid crystals.

References

[1] C.H.N. Yuen, R.F. Martinez-Botas, Film cooling characteristics of a single round hole at various angles in a crossflow: part II heat transfer coefficients. PII: S0017-9310(02)00273-9.
[2] V.L. Eriksen, R.J. Goldstein, Heat transfer and film cooling following injection through inclined circular tubes, ASME J. Heat Transfer (1974) 239–245.
[3] R.J. Goldstein, T. Yoshida, Boundary layer and laminar injection on film cooling performance, ASME J. Heat Transfer 104 (1982) 355–362.
[4] R.J. Goldstein, P. Jin, R.L. Olson, Film cooling effectiveness and mass/heat transfer coefficient downstream of one row of discrete holes, ASME Paper No. 98-GT-174, 1998.
[5] G. Bergeles, Three-dimensional discrete hole cooling processes: an experimental and theoretical study, Ph.D. thesis, University of London, Imperial College of Science, Technology and Medicine, London, 1976.
[6] A. Brown, C.L. Saluja, Film cooling from a single hole and a row of holes of variable pitch to diameter ratio, Int. J. Heat Mass Transfer 22 (1979) 525–533.
[7] A.K. Sinha, D.G. Bogard, M.E. Crawford, Film-cooling effectiveness downstream of a single row of holes with variable density ratio, ASME J. Turbomach. 113 (1991) 442–449.
[8] D.L. Schmidt, B. Sen, D.G. Bogard, Film cooling with compound angle holes: adiabatic effectiveness, ASME J. Turbomach. 118 (1996) 807–813.
[9] J.F. Keffer, W.D. Baines, The round turbulent jet in a cross wind, J. Fluid Mech. (15) (1962) 481–496.
[10] J.W. Ramsey, R.J. Goldstein, Interaction of a heated jet with a deflecting stream, ASME J. Heat Transfer 93 (1971) 365–372.
[11] Z. Moussa, J.W. Trischka, S. Eskinazi, The near field in the mixing of a round jet with a cross-stream, J. Fluid Mech. 80 (1977) 49–80.
[12] J. Andreopoulos, Heat transfer measurements in a heated jet-pipe issuing into a cold cross stream, Am. Inst. Phys. Phys. Fluids 26 (1983) 3201–3210.
[13] J. Andreopoulos, On the structure of jets in a crossflow, J. Fluid Mech. 157 (1985) 163–197.
[14] R. Flack, K. Dullenkopf, V. Scherer, Constituency measurements in the mixing region of a cross flow jet using laser velocimeter, Exp. Fluids 17 (1994) 198–204.
[15] T.F. Fric, A. Roshko, Vortical structures in the wake of a transverse jet, J. Fluid Mech. 279 (1994) 1–47.
[16] R.M. Kelso, A.J. Smits, Horseshoe vortex systems resulting from the interaction between a laminar boundary layer and a transverse jet, Am. Inst. Phys. Phys. Fluids 7 (1995) 153–158.
[17] R.M. Kelso, T.T. Lim, A.E. Perry, An experimental study of round jets in cross-flow, J. Fluid Mech. 306 (1996) 111–144.
[18] V.S. Sivadas, B.S. Pani, G.E. Bütefisch, G.E.A. Meier, Flow visualisation studies on growth of area of deflected jets, Exp. Fluids 23 (2) (1997) 105–112.
[19] R.J. Margason, Fifty years of jet in crossflow research, AGARD Meeting on Computational and Experimental Assessment of Jets in Crossflow, April 1993.
[20] J. Andreopoulos, W. Rodi, An experimental investigation of jets in crossflow, J. Fluid Mech. 138 (1984) 93–127.
[21] G. Bergeles, A.D. Gosman, J. Launder, The near-field character of a jet discharged normal to a mainstream, ASME J. Heat Transfer 98 (1976) 373–378.
[22] D. Crabb, D.F.G. Durao, J.H. Whitelaw, A round jet normal to a crossflow, ASME J. Fluids Eng. 103 (1981) 142–153.
[23] D.K. Walters, J.H. Leylek, A detailed analysis of film cooling physics: part I—streamwise injection with cylindrical holes, ASME J. Turbomach. 122 (2000) 102–112.
[24] S.W. Lee, J.S. Lee, S.T. Ro, Experimental study on the flow characteristics of streamwise inclined jets in crossflow, ASME J. Turbomach. 116 (1994) 97–105.
[25] J.R. Pietrzyk, D.G. Bogard, M.E. Crawford, Hydrodynamics measurements of jets in crossflow for gas turbine film cooling applications, AMSE J. Turbomach. 111 (2) (1989) 139–145.
[26] J.R. Pietrzyk, D.G. Bogard, M.E. Crawford, Effects of density ratio on the hydrodynamcis of film cooling, Trans. AMSE J. Turbomach. 112 (2) (1990) 437–443.
[27] J.W. Baughn, Liquid crystal methods for studying turbulent heat transfer, Int. J. Heat Fluid Flow 16 (5) (1995) 365–375.

[28] P.T. Ireland, T.V. Jones, The measurement of local heat transfer coefficients in blade cooling geometries, AGARD Conference Proceedings on Heat Transfer and Cooling, CP 390 Paper 28, 1985.
[29] R.S. Bunker, D.E. Metzger, S. Wittig, Local heat transfer in turbine disk cavities. Part I: rotor and stator cooling with hub injection of coolant, ASME J. Turbomach. 114 (1992) 211–220.
[30] Z. Wang, P.T. Ireland, T.V. Jones, An advanced method of processing liquid crystal video signals from transient heat transfer experiments, ASME J. Turbomach. 117 (1995) 184–189.
[31] R.J. Vedula, D.E. Metzger, A method for the simultaneous determination of local effectiveness and heat transfer distributions in three-temperature convection situations, ASME Paper No. 91-GT-345, 1991.
[32] S.V. Ekkad, J.C. Han, Flat plate film cooling effectiveness and heat transfer using a transient liquid crystal technique, Proc. ASME/JSME Thermal Eng. Conf. 3 (1995) 445–452.
[33] K.W. Van Treuren, Z. Wang, P.T. Ireland, T.V. Jones, Application of the transient liquid crystal technique to measure heat transfer and adiabatic wall temperature beneath and array of impinging jets, Proc. Eurotherm 32 (1993) 82–86.
[34] H. Babinsky, J.A. Edwards, Automatic liquid crystal thermography for transient heat transfer measurements in hypersonic flow, Exp. Fluids 21 (1996) 227–236.
[35] C.H.N. Yuen, Measurement of local heat transfer coefficient and film cooling effectiveness ion film cooling geometries, Ph.D. thesis, University of London, Imperial College of Science, Technology and Medicine, London, 2000.
[36] D.J. Farina, J.M. Hacker, R.J. Moffat, J.K. Eaton, Illuminant invariant calibration of thermochromic liquid crystals, Visual. Heat Transfer Proc., ASME HTD 252 (1993) 1–11.
[37] S.J. Kline, F.A. McClintock, Describing uncertainties in single-sample experiments, Mech. Eng. (1953) 3–8.
[38] P.J. Schneider, in: Conduction Heat Transfer, 6th ed., Addison-Wesley, Reading, Mass, 1974, pp. 176–181.
[39] D.E. Metzger, H.J. Carper, L.R. Swank, Heat transfer with film cooling near non-tangential injection slots, J. Eng. Power 90 (1968) 157–163.
[40] R.J. Goldstein, E.R.G. Eckert, J.W. Ramsey, Film cooling with injection through holes: adiabatic wall temperatures downstream of a circular hole, ASME J. Eng. Power (1968) 384–395.
[41] V.L. Eriksen, Film cooling effectiveness and heat transfer with injection through holes, Ph.D. thesis, University of Minnesota, 1971.
[42] R.J. Goldstein, E.R.G. Eckert, V.L. Eriksen, J.W. Ramsey, Film cooling following injection through inclined circular tubes, Isr. J. Technol. 8 (1970) 145–154.
[43] K. Kadotani, R.J. Goldstein, Effects of mainstream variables on jet issuing from a row of inclined holes, ASME J. Eng. Power 101 (2) (1979) 298–304.
[44] A.L. Brundage, M.W. Plesniak, S. Ramadhyani, Influence of coolant feed direction and hole length on film cooling jet velocity profiles, ASME Paper No. 99-GT-35, 1999.